

# RSC Advances



This is an *Accepted Manuscript*, which has been through the Royal Society of Chemistry peer review process and has been accepted for publication.

*Accepted Manuscripts* are published online shortly after acceptance, before technical editing, formatting and proof reading. Using this free service, authors can make their results available to the community, in citable form, before we publish the edited article. This *Accepted Manuscript* will be replaced by the edited, formatted and paginated article as soon as this is available.

You can find more information about *Accepted Manuscripts* in the [Information for Authors](#).

Please note that technical editing may introduce minor changes to the text and/or graphics, which may alter content. The journal's standard [Terms & Conditions](#) and the [Ethical guidelines](#) still apply. In no event shall the Royal Society of Chemistry be held responsible for any errors or omissions in this *Accepted Manuscript* or any consequences arising from the use of any information it contains.

## Synthesis and Structure-property Investigation of Multi-arm Oligothiophenes

Choong Ping Sen, and Suresh Valiyaveetil\*

Received 00th January 20xx,  
Accepted 00th January 20xx

DOI: 10.1039/x0xx00000x

www.rsc.org/

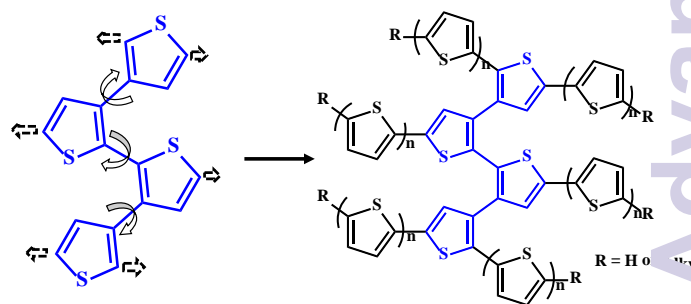
Oligothiophenes are used in many applications owing to their easy accessibility in high purity, tunable electron density, high chemical stability and desired processability in solution and in solid state. In this work, a series of soluble branched oligothiophenes have been synthesized and fully characterized. The target molecules (**SCT-1** to **SCT-4**) are soluble in common organic solvents. Full characterization of optical and electrochemical properties indicated that the extended  $\pi$ -conjugation led to red-shifts in absorption maximum ( $\lambda_{\text{max}}$ ) from 360 nm (**SCT-1**) to 440 nm (**SCT-4**). Fluorescence quantum yields were in the range of 6 – 45% for the **SCTs**. The observed properties of the target molecules are better than the corresponding linear oligothiophenes. Electron deficient Hg(II) cations interact with electron rich **SCT-4** to form charge transfer complex which led to significant quenching of photoluminescence in solution. Moreover, electron deficient molecule, 7,7,8,8-tetracyanoquinodimethane (TCNQ), also interact with electron rich **SCTs** to form TCNQ dianion (TCNQ<sup>2-</sup>). Such conjugated optical materials could be used for developing potential applications in the near future.

### Introduction

One-dimensional or multidimensional oligothiophenes have been synthesized and used in optoelectronic applications such as organic solar cells (OSCs),<sup>1,2</sup> light emitting diodes (OLEDs),<sup>3</sup> sensors<sup>4</sup> and field effect transistors (OFETs)<sup>5–8</sup> owing to their excellent chemical stability, high hole mobility, tunable optoelectronic properties and accessibility of high purity materials as compared to their polymeric counterparts.<sup>9</sup> High crystallinity of oligothiophenes results in improved performance of devices owing to enhanced charge transport,<sup>10</sup> but leads to poor solubility and low processability. Solubilizing groups such as alkyl chains are commonly attached on oligothiophenes for enhancing the solubility in common organic solvents.<sup>11,12</sup> In addition, bulky groups or multidimensional architectures hinders the formation of face to face  $\pi$ -dimers, which is useful for understanding the charge transport mechanism.<sup>13</sup> Multi-dimensional oligothiophenes with star-,<sup>14</sup> H-shaped,<sup>15</sup> spiro-,<sup>16</sup> and dendrimeric architectures<sup>17</sup> have been synthesized and applied in various applications. The increased dimensionality of the conjugated oligothiophene is found to exhibit isotropic charge transport as compared to that in linear oligothiophenes,<sup>18</sup> which could be advantageous in order to obtain a higher charge carrier mobility in devices. Recently, 3-D swivel cruciform oligothiophene dimers have shown an improved solubility in

organic solvent due to high degree of rotational freedom between two linear oligothiophenes.<sup>19,20</sup> Design and synthesis of oligothiophenes with interesting architectures are needed to improve intrinsic electronic and transport properties.<sup>21,22</sup>

Herein, we design and synthesize a series of new multi-branched oligothiophenes (**SCTs**) based on a quaterthiophene backbone with extended conjugation (Scheme 1). The correlation between the structures of **SCTs** with observed optical properties is investigated using absorption and photoluminescence spectroscopy. These highly branched **SCTs** are easy to prepare and structurally defined. In addition, high solubility and processability are expected in **SCTs** as compared to their linear oligothiophene analogues. The conformations of the molecules are established using optical studies in solution and in solid state.



**Scheme 1.** Design strategy and general structure of the target molecules.

Department of Chemistry, 3 Science Drive 3, National University of Singapore, Singapore-117543. E-mail: chmsv@nus.edu.sg

Electronic Supplementary Information (ESI) available: [<sup>1</sup>H and <sup>13</sup>C NMR spectra, mass spectra, absorption and photoluminescence spectra, DFT optimized geometries and SEM images of all compounds]. See DOI: 10.1039/x0xx00000x

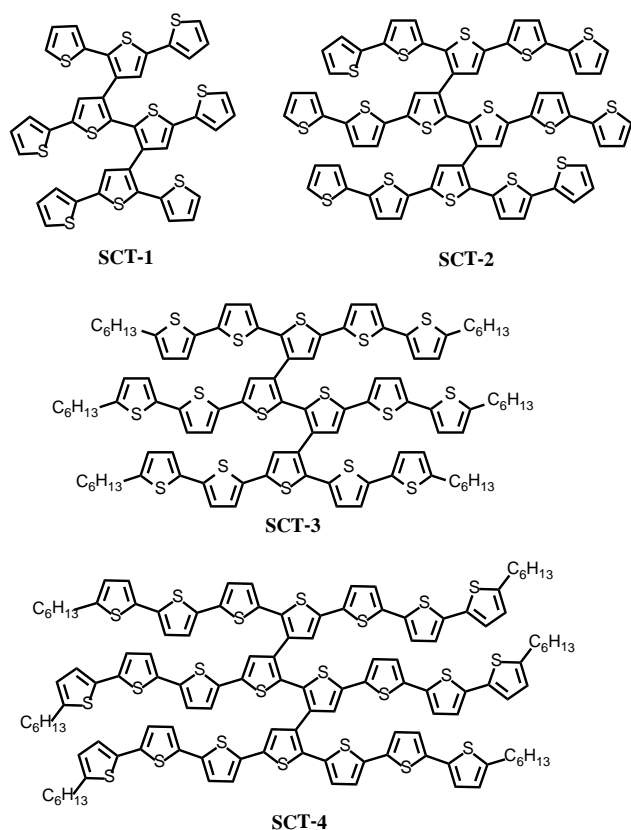


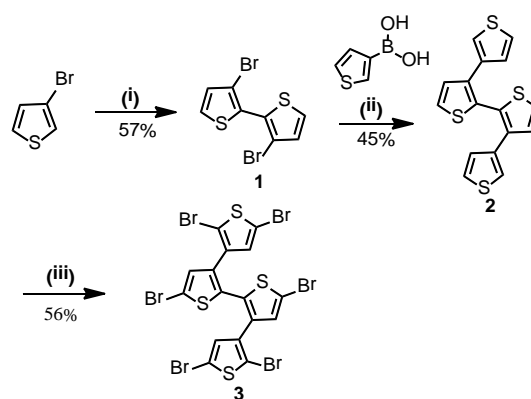
**Figure 1.** Molecular structures of the target 3D oligothiophene molecules (SCT-1 to SCT-4).

## Results and Discussion

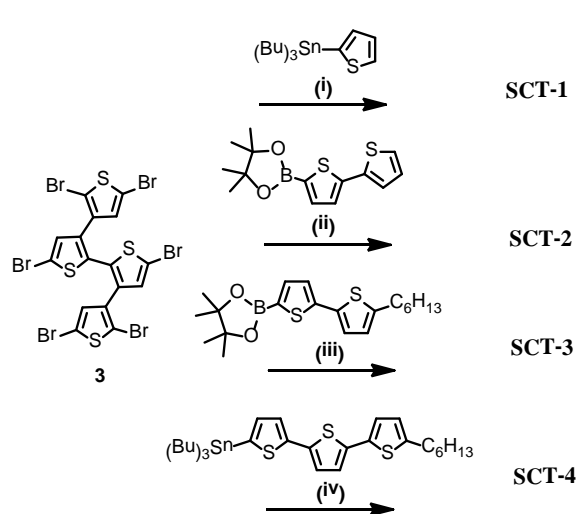
Target molecules, **SCT-1** to **SCT-4** (Figure 1) were synthesized using the routes given in Schemes 2 and 3 and fully characterized.

### Synthesis and characterization

Synthesis of the hexabrominated central quaterthiophene is given in Scheme 2. 3,3'-Dibromo-2,2'-bithiophene (**1**) was prepared by lithiating commercially available 3-bromothiophene with lithium diisopropylamide (LDA) followed by  $\text{CuCl}_2$ -oxidative homocoupling to obtain the product in 57% yield.<sup>23</sup> The palladium-catalyzed Suzuki-Miyaura cross-coupling between **1** and 2.2 equivalents of 3-thienyl boronic acid afforded 3,3':2',2'':3'',3''''-quaterthiophene **2** in 45% yield.<sup>24</sup> Bromination of **2** with 12 equivalents of NBS in  $\text{CHCl}_3/\text{AcOH}$  at 80 °C afforded 2,2''',5,5'',5''',5''''-hexabromo-3,3':2',2'':3'',3''''-quaterthiophene **3** in 56% yield, which was used as a central building block for synthesizing the target molecules. **SCT-1**, **SCT-2**, **SCT-3** and **SCT-4** were synthesized using Stille or Suzuki-Miyaura palladium-catalyzed cross-coupling reactions with the corresponding stannylated or borylated oligothiophenes in good yields (Scheme 3). Alkyl chains are introduced in larger molecules to enhance the solubility.



**Scheme 2.** Synthesis of quaterthiophene trimer backbone; (i) LDA, THF, -78 °C, 1 h; (b)  $\text{CuCl}_2$ , -78 °C, 10 mins; (ii)  $\text{Pd}(\text{PPh}_3)_4$ ,  $\text{K}_2\text{CO}_3$ , THF/ $\text{H}_2\text{O}$ , 70 °C, 24 h; (iii) NBS,  $\text{CHCl}_3/\text{AcOH}$ , 80 °C, 4 h.



**Scheme 3.** Synthesis of **SCTs** by Stille or Suzuki cross coupling reaction; (i)  $\text{Pd}(\text{PPh}_3)_4$ , THF, 70 °C, 38 h; (ii)  $\text{Pd}(\text{PPh}_3)_4$ ,  $\text{K}_2\text{CO}_3$ , THF/ $\text{H}_2\text{O}$ , 70 °C, 38 h; (iii)  $\text{Pd}(\text{PPh}_3)_4$ ,  $\text{K}_2\text{CO}_3$ , THF/ $\text{H}_2\text{O}$ , 70 °C, 48 h; (iv)  $\text{Pd}(\text{PPh}_3)_4$ , THF, 70 °C, 48 h.

Solubility of **SCT-2** is poor in THF and chloroform, hence six hexyl groups were introduced at the terminal  $\alpha$ -positions of the **SCT-3** to improve the solubility. As expected, both **SCT-1** (small molecule with sufficient flexibility) and **SCT-3** are highly soluble in common organic solvents. This allowed us to fully characterize the molecular structures of intermediates and **SCTs** using  $^1\text{H}$  and  $^{13}\text{C}$  NMR spectroscopy, mass spectrometry and elemental analysis (ESI, Figure S1 – S18).

### Thermal stabilities of SCTs

In order to understand the thermal stability of the compounds, thermogravimetric analyses (TGA) and differential scanning calorimetry (DSC) of all **SCTs** were conducted under nitrogen atmosphere. The observed TGA traces indicated high thermal stability with only 5% weight loss before 430 °C, 500 °C, 400 °C and 380 °C for **SCT-1**, **SCT-2**, **SCT-3** and **SCT-4**, respectively (Figure 2).

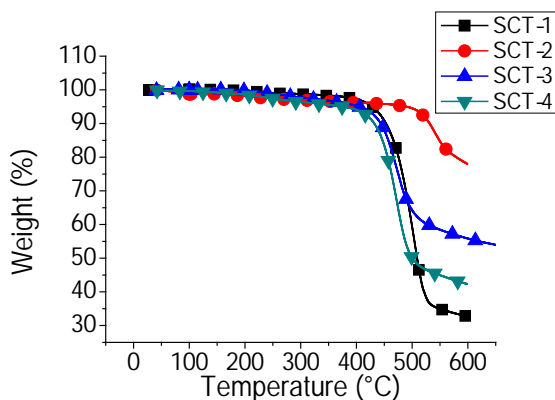


**Figure 2.** TGA traces on SCTs recorded at heating rate of 10 °C min<sup>-1</sup> under nitrogen atmosphere.

**SCT-2** has higher melting point (270 °C) and decomposition temperature (492 °C) than **SCT-1** owing to the better  $\pi$ -stacking as oligothiophene length increases. In contrast to **SCT-1**, which showed a reversible melting and crystallization (215 °C), **SCT-2** did not crystallize upon cooling from the melt. However, an exothermic peak at 235 °C was observed during second heating, which corresponded to recrystallization of **SCT-2**. Both melting point (155 °C) and decomposition temperature (405 °C) of alkylated **SCT-3** are lower than unsubstituted **SCT-2**. This is explained by disruption of intermolecular interaction in **SCT-3** with six hexyl groups. **SCT-3** showed a slow crystallization at 60 °C during cooling process. A higher melting point (250 °C) was observed in **SCT-4** with longer oligothiophene length as compared to **SCT-3** (155 °C). On the other hand, the decomposition temperature of **SCT-4** (390 °C) is not significantly different from **SCT-3** (405 °C), which could be due to a more rigid conformation of **SCT-4**. All thermal properties of SCTs are summarized in Table 1.

### Photophysical properties of SCTs

Absorption spectra of SCTs were recorded in THF at room temperature (Figure 3). The maximum absorption wavelengths were red-shifted as number of thiophene moieties increases in the structure of **SCT-1** to **SCT-4**. Such trend was also observed for linear oligothiophenes with progressive extension in  $\pi$ -conjugation.<sup>25</sup> A red-shift (5 nm) in absorption maximum was observed for **SCT-1** (360 nm) as compared to linear unsubstituted terthiophene analogues (355 nm, CHCl<sub>3</sub>)<sup>26</sup> and a blue shift in absorption maximum as compared to linear quaterthiophene analogue (390 nm, CHCl<sub>3</sub>).<sup>26</sup> This is expected due to the twisted conformation and disruption in  $\pi$ -conjugation. The absorption maxima of SCTs are influenced by the number of thiophene moieties present on the side chains. In the case of **SCT-2** and **SCT-3**, the absorption maxima are similar to the linear pentathiophenes (410 nm, CHCl<sub>3</sub>).<sup>27</sup> The absorption maximum of **SCT-4** (440 nm) is comparable to the  $\alpha$ -connected linear heptathiophenes.<sup>28</sup> In addition, the absorption band edge has shifted to longer wavelength from

**Table 1.** Summary of thermal properties of SCTs.

	Decomposition Temperature °C <sup>a</sup>	Melting Point °C <sup>b</sup>
<b>SCT-1</b>	430	230
<b>SCT-2</b>	492	270
<b>SCT-3</b>	406	155
<b>SCT-4</b>	390	250

<sup>a</sup> Decomposition temperature was measured at 5% weight degradation of SCTs under nitrogen atmosphere using TGA. <sup>b</sup> Melting point was determined at the maximum of endothermic peak observed in DSC thermograms.

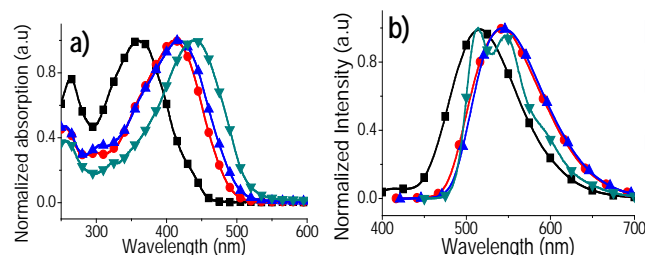


**Figure 3.** UV-vis absorption spectra (a) and photoluminescence spectra (b) of **SCT-1** (■), **SCT-2** (●), **SCT-3** (▲) and **SCT-4** (▼) in THF.

**SCT-1** (453 nm) to **SCT-4** (533 nm) in THF, indicating an extended  $\pi$ -conjugated system in **SCT-4**. The emission wavelengths for **SCT-1**, **SCT-2**, **SCT-3** and **SCT-4** are 516 nm, 542 nm, 542 nm and 550 nm, respectively. The largest stoke shift observed in **SCT-1** suggests a significant conformational change between ground and excited state (Table 2). As the number of thiophene rings increases in **SCT-1** to **SCT-4**, the torsional motion becomes smaller owing to the extended oligothiophene length in the system. Thus a smaller Stoke shift is expected in a more rigid **SCT-4**. In addition, enhanced photoluminescence was observed from more conjugated larger SCTs. The fluorescence quantum yields of **SCT-1**, **SCT-2**, **SCT-3** and **SCT-4** in THF were determined as 6 %, 11.1 %, 11.4 % and 46.6 %, respectively, with reference to fluorescein (0.1 M NaOH, quantum yield of 0.85). Moreover, higher molar extinction coefficient was observed with increasing conjugation length from **SCT-1** to **SCT-4**. The absorption spectra of SCTs films were recorded to investigate the change in absorption maximum and absorption edge from solution to solid state. The SCT films were prepared by spin casting the solutions of SCTs in THF at room temperature. Red shifts in absorption maxima were observed for **SCT-1** (20 nm), **SCT-2** (28 nm), and **SCT-3** (17 nm) after comparing the values from solution spectra with those obtained from solid state spectra (Figure 4). Similarly, red shifts in absorption edges for **SCT-1** (31 nm), **SCT-2** (45 nm), and **SCT-3** (50 nm) were also observed after comparing the solution spectra with solid state spectra.

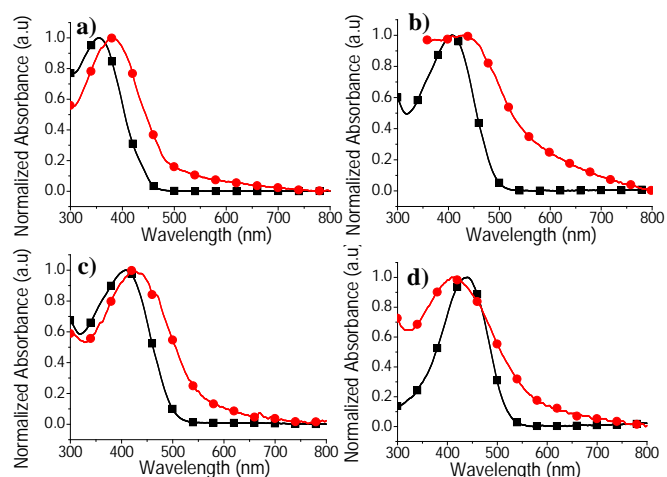


**Figure 4.** Comparison of absorption spectra of (a) **SCT-1**, (b) **SCT-2**, (c) **SCT-3** and (d) **SCT-4** in THF (■) and spin-casted films (●) on quartz plate at room temperature.

**Table 2.** Photophysical properties of **SCT-1**, **SCT-2**, **SCT-3** and **SCT-4**

	$\lambda_{\text{max}}^{\text{a}}$ nm	$\epsilon^{\text{b}} \cdot 10^5$ $\text{cm}^{-1}\text{M}^{-1}$	$\lambda_{\text{onset}}^{\text{c}}$ nm	$\lambda_{\text{max}}^{\text{d}}$ nm	$\lambda_{\text{onset}}^{\text{c}}$ nm	$E_{\text{g}}^{\text{e}}$ eV	$\lambda_{\text{em}}^{\text{f}}$ nm	$\phi_{\text{f}}^{\text{g}}$ %
<b>SCT-1</b>	360	0.49	453	380	484	2.56	516	6.0
<b>SCT-2</b>	410	1.01	500	438	545	2.28	542	11.1
<b>SCT-3</b>	413	1.03	505	430	555	2.23	542	11.4
<b>SCT-4</b>	440	1.44	533	413	545	2.27	515, 550	46.6

<sup>a</sup> Recorded in THF. <sup>b</sup>  $\epsilon$  extinction coefficient was calculated by dividing absorbance with concentration and cuvette path length. <sup>c</sup>  $\lambda_{\text{onset}}$  was calculated from the intersection of the tangent lines drawn to the lowest energy absorption edge to the baseline. <sup>d</sup>  $\lambda_{\text{max}}$  was measured from spin-casted thin film on quartz plate. <sup>e</sup>  $E_{\text{g}} = 1240 / \lambda_{\text{onset thin film}}$ . <sup>f</sup> Steady state photoluminescence recorded in THF. <sup>g</sup>  $\phi_{\text{f}}$  fluorescence quantum yields were determined in THF using fluorescein (0.1 M NaOH, quantum yield of 0.85) as reference.

In contrast, absorption maximum of **SCT-4** in thin films shows a blue-shift (27 nm) and a broad peak. Even though, the absorption edge of **SCT-4** in solid state is red-shifted to longer wavelength, the magnitude of red-shift (12 nm) is significantly smaller as compared to other **SCTs**, and linear oligothiophenes. Therefore it is conceivable that **SCT-4** does not adopt a planar conformation in solid state owing to the steric hindrance from side arms. The band gap energies were calculated to be 2.56 eV, 2.28 eV, 2.23 eV, and 2.27 eV for **SCT-1**, **SCT-2**, **SCT-3**, and **SCT-4**, respectively. All photophysical properties are summarized in Table 2.

All **SCT** molecules are photochemically stable under ambient conditions, both in solution and thin film. The photochemical stability of **SCTs** molecules was evaluated based on changes in

absorption and emission profile after photoirradiation. No changes in absorption or emission maxima and intensities were observed for all **SCTs** molecules, both in solution and in thin film. To further test the photochemical stability of **SCTs**, high intensity light source (50 Watt white LED light, 15 cm distance between light source and substrates) was used for continuous irradiation on **SCT** molecules in dilute THF at ambient conditions. **SCT-1** showed no changes in absorption and emission intensities after 24 hours of irradiation (ESI, Figure S31-32). In contrast, the absorption maximum of **SCT-2** had shifted to shorter wavelength with 13% loss of emission intensity after 24 hours. Similarly, the absorption maximum of **SCT-3** also shifted to shorter wavelength with 10% loss of emission intensity after 24 hours. In the case of **SCT-4**, the absorbance and emission intensity were decreased by 5% and 7%, respectively. The spin-casted films of **SCTs** were tested under exact conditions (ESI, Figure S33-34). **SCT-1** showed 23% and 56% decrease in absorbance and emission intensity, respectively. The absorbance and emission intensities of **SCT-2** thin film were decreased by 23% and 43%, respectively after 24 hours. In contrast, **SCT-3** showed a blue shift in absorption maximum and 88% loss in emission intensity. On the other hand, **SCT-4** showed 53% and 70% decreases in absorbance and emission intensities, respectively. This suggested that the **SCT-3** and **SCT-4** are more photochemically unstable owing to their high HOMO energy level.

#### Electrochemical properties and theoretical computation of **SCTs**

Cyclic voltammetry (CV) was used to probe the redox behaviors of **SCTs** in thin films and in dichloromethane solution (Figure 5). The CV scans of thin film were recorded in 0.1 M n-Bu<sub>4</sub>NPF<sub>6</sub> solution in anhydrous acetonitrile and **SCTs** dissolved in dichloromethane solution with 0.1 M n-Bu<sub>4</sub>NPF<sub>6</sub> solution using a scan rate of 100 mV s<sup>-1</sup> and a standard calomel electrode (SCE) as reference electrode. The HOMO energy levels of **SCTs** were estimated from the onset oxidation and calibrated with ferrocene/ferrocenium (Fc/Fc<sup>+</sup>) redox couple as internal reference. In thin film, **SCT-1** shows one partial reversible oxidation peak E<sub>ox,1</sub> at 0.65 V corresponding to the formation of oligothiophene cation radical of terthiophene.<sup>26</sup> Absence of quaterthiophene oxidation/reduction peaks in CV indicates minimal electronic interaction between oligothiophene arms of the same molecule. In the more extended conjugated **SCT-2**, there are two oxidation peaks E<sub>ox,1</sub> and E<sub>ox,2</sub> at 0.53 and 0.91 V owing to the formation of monocation and dication. The first oxidation peak in **SCT-2** has shifted to a lower positive potential owing to the formation of cation on an extended oligothiophene unit. Similarly, **SCT-3** showed two oxidation peaks E<sub>ox,1</sub> and E<sub>ox,2</sub> at 0.57 V and 0.76 V. The CV traces of **SCT-4** show three oxidation processes at 0.38 V, 0.61 V and 0.91 V. However, formation of a radical cation on single oligothiophene of **SCT-4** would be unstable. Therefore it is conceivable that the three oxidation processes correspond to the formation of three different radical cations on three independent oligothiophene arms of **SCT-4**.

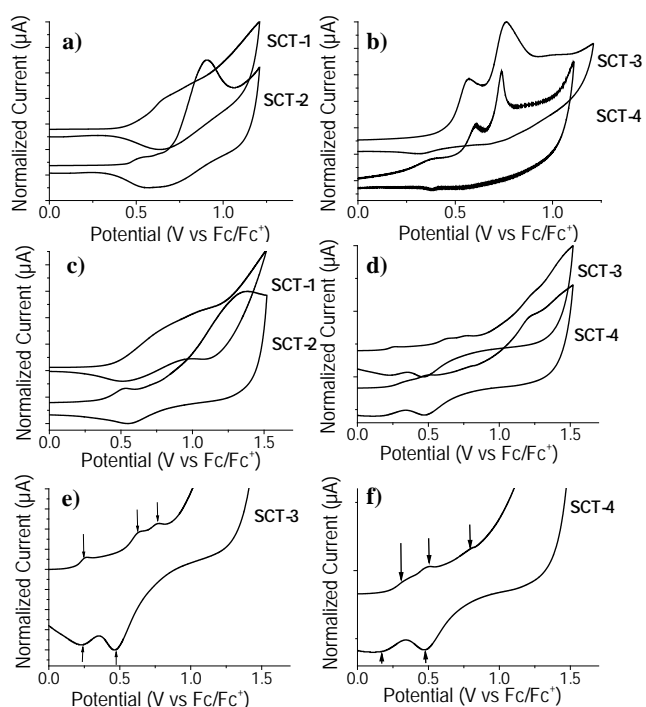


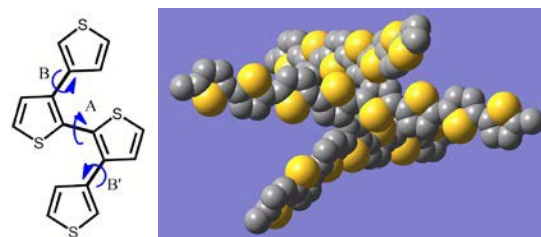
**Figure 5.** Cyclic voltammograms of SCTs measured in thin film (a and b) and in anhydrous dichloromethane (c and d) at a rate of  $100 \text{ mV s}^{-1}$ . The magnified cyclic voltammograms of SCT-3 (e) and SCT-4 (f) in dichloromethane to show the respective oxidation and reduction processes. The SCTs films were prepared by drop casting THF solutions of SCTs on Pt disk electrode. For thin films studies, a  $0.1 \text{ M n-Bu}_4\text{NPF}_6$  in anhydrous acetonitrile was used as supporting electrolyte. For solution state studies, a  $0.1 \text{ M n-Bu}_4\text{NPF}_6$  in anhydrous dichloromethane was used as supporting electrolyte. All voltammograms were calibrated against ferrocene/ferrocenium ion redox couple.

**Table 3.** Summary of electrochemical properties of SCTs.

SCT-	$E_{\text{ox},1}$ film	$E_{\text{ox},2}$ film	$E_{\text{ox},3}$ film	HOM $O^{\text{a}}$ film (eV)	$E_{\text{ox},1}$ dcm	$E_{\text{ox},2}$ dcm	$E_{\text{ox},3}$ dcm	HOM $O^{\text{b}}$ dcm (eV)
1	0.65	-	-	-5.28	0.70	-	-	-5.32
2	0.53	0.91	-	-5.26	0.52	-	-	-5.20
3	0.57	0.76	-	-5.22	0.26	0.63	0.77	-5.05
4	0.38	0.61	0.91	-5.07	0.31	0.50	0.79	-5.03

<sup>a</sup> Electrochemical HOMO of SCTs thin films =  $-(E^{\text{ox}} + 4.8) \text{ eV}$ , where  $E^{\text{ox}}$  was determined from the onset potentials of first oxidation peak calibrated with ferrocene/ferrocenium ion redox couple. <sup>b</sup> Electrochemical HOMO of SCTs in dichloromethane =  $-(E^{\text{ox}} + 4.8) \text{ eV}$ , where  $E^{\text{ox}}$  was determined from the onset potentials of first oxidation peak calibrated with ferrocene/ferrocenium ion redox couple.

In comparison to CV traces in thin films, the SCTs in dichloromethane showed a more pronounced reversibility of the oxidation processes. SCT-3 and SCT-4 showed multiple oxidation processes with partial reversibility (Figure 5c-f). All HOMO and LUMO energy levels of SCTs are calculated and summarized in Table 3.



	SCT-1	SCT-2	SCT-3	SCT-4
$A^\circ$	36.9	32.8	36.5	36.1
$B^\circ$	55.7	63.2	58.5	56.6
$B'^\circ$	55.7	62.8	59.5	58.8

**Figure 6.** Dihedral angles between thiophene rings in SCTs were calculated using DFT and the space-filling molecular representation of SCT-4 optimized at B3LYP/6-31G(d) level. Hydrogen atoms were omitted for better clarity.

The optimized structures and Frontier Orbital energy levels of SCTs were calculated using density functional theory (DFT) at B3LYP/6-31G(d) level (ESI, Figure S21-30). For example in SCT-4, the dihedral angle between the planes involving end thiophene and center bithiophene moiety (A) is  $36.1^\circ$  while the dihedral angles between side thiophene and center bithiophene (B and B') are  $56.6^\circ$  and  $58.8^\circ$ , respectively (Figure 6). All SCT molecules have a swivel-type conformation where three oligothiophene chains are pointing in different directions. Moreover, the out-of-plane conformation of all three branches led to inefficient orbital overlapping as compared to that found in linear oligothiophenes, which is in good agreement with the results obtained from optical and electrochemical studies. The theoretical HOMO energy levels of SCTs are higher than the one estimated using the data from CV in solid state or solution state (ESI, see Table S1). This could be due to the twisted structural conformation, which leads to inefficient orbital overlapping. Nevertheless, SCTs follow the same trend, where the HOMO energy levels are increased with decreased band gaps. In addition, the HOMO and LUMO electron densities are distributed evenly in all three oligothiophene branches of SCTs.

### Morphology of SCTs

Precipitation of SCTs was carried out using slow evaporation of dilute solution in THF- $\text{H}_2\text{O}$  mixture over two days. The resulting suspension was dropcasted on a glass substrate and dried at ambient condition. Field effect scanning electron microscopy (SEM) was used to examine the morphology of solid precipitate obtained from all SCTs. SEM micrographs of SCT-1 showed formation of microspheres with a diameter in the range of  $0.5 \mu\text{m}$  to  $2 \mu\text{m}$ . Slow evaporation of THF solution allows SCT-2 to form crystalline needle-like rods with an average width of  $2 \mu\text{m}$  and up to a few millimeters in length. In contrast, SCT-3 with solubilizing hexyl groups formed nanosized spherical particles with an average diameter of  $1.0 \mu\text{m}$ .

nm, while **SCT-4** formed random shapes under similar conditions (Figure 7).

### Interaction of SCTs with Hg(II) cations

It is well-known that Pb(II), Cd(II) and Hg(II) cations show strong affinity for sulfur containing groups such as thiol. Even though, thiophene-metal ion interactions are expected to be weak, thiophene groups from adjacent chains are able to interact with metal ions owing to the structural rigidity and orientation of S atoms of thiophene rings in **SCTs**. The complexation between thiophene derivatives and Hg(II) cation for sensor application has been reported.<sup>29,30</sup> Our study was focused towards understanding the interaction between thienyl sulfur atoms of **SCTs** and heavy metal ions for potential application such as sensor. The interaction of heavy metal ions with **SCTs** was investigated using absorption spectroscopy and photoluminescence. It is found that Pb(II) and Cd(II) cations did not change absorption and emission profiles of **SCTs** (ESI, Figure S35). On the other hand, Hg(II) ions showed significant changes in the absorption and emission maxima of **SCTs**. Both absorbance and emission intensities were decreased upon addition of Hg(II) ions to the solution of **SCTs** in THF (Figure 8 and 9). Particularly, formation of yellow precipitate was observed when excess Hg(II) ions was added into **SCT-4** in THF, resulting in disappearance of absorption and quenching of emission intensity of the solution. This indicates a strong interaction of **SCT-4** with Hg(II) ions.

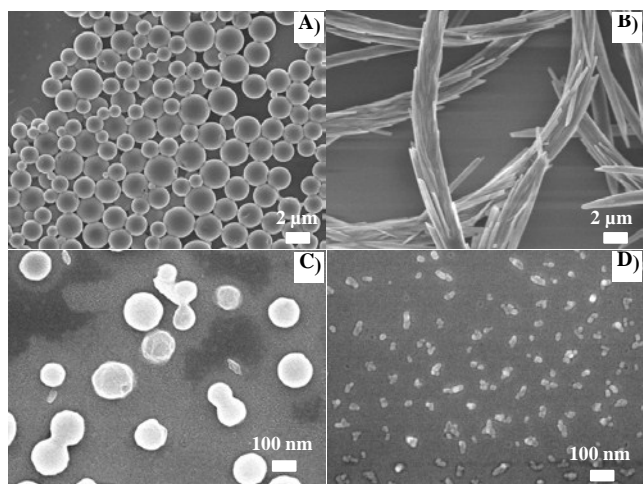


**Figure 7.** SEM micrographs of **SCT-1** (A), **SCT-2** (B), **SCT-3** (C) and **SCT-4** (D); **SCTs** in THF were added slowly to H<sub>2</sub>O in a glass vial with screw cap. The above solution was left at room temperature for two days. The resulting **SCTs** suspension was drop casted on a glass substrate and dried under ambient condition before SEM imaging.

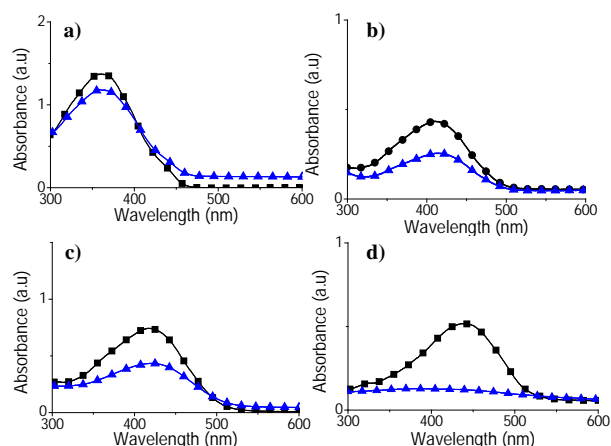


**Figure 8.** Absorption spectra of (a) **SCT-1**, (b) **SCT-2**, (c) **SCT-3** and (d) **SCT-4** in THF before (■) and after (▲) addition of aqueous Hg(OAc)<sub>2</sub> solution ( $1 \times 10^{-3}$  M).

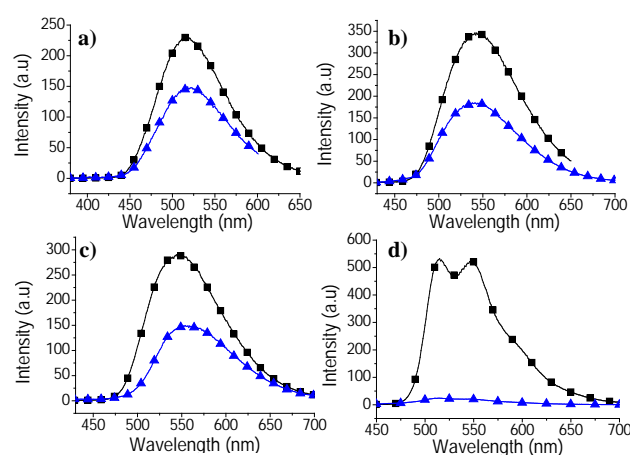


**Figure 9.** Photoluminescence spectra of (a) **SCT-1**, (b) **SCT-2**, (c) **SCT-3** and (d) **SCT-4** in THF before (■) and after (▲) addition of aqueous Hg(OAc)<sub>2</sub> solution ( $1 \times 10^{-3}$  M).

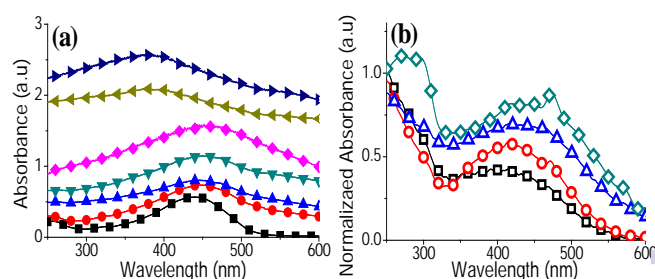


**Figure 10.** (a) Absorption spectra of **SCT-4** (-■-) in presence of Hg(II) ions (600 eq (-●-), 1200 eq (-▲-), 1800 eq (-▼-), 2400 eq (-◆-), 3000 eq (-◀-), 3600 eq (-▶-)) in THF/H<sub>2</sub>O; and (b) absorption spectra of SCTs-Hg solid, **SCT-1**/Hg (-□-), **SCT-2**/Hg (-○-), **SCT-3**/Hg (-△-), and **SCT-4**/Hg (-◇-).

The concentration dependent study was carried out by titrating the **SCT-4** solution in THF with Hg(II) ion (Figure 10a), to understand the absorption changes with respect to the

Hg(II) ion concentration. The absorption maximum of **SCT-4** was shifted from 440 nm to 458 nm upon increase in concentration of Hg(II) ions. Such observation could be attributed to the formation of **SCT-4**/Hg complexes.<sup>31</sup> Increasing the concentration of Hg(II) ions further led to precipitation of **SCT-4**/Hg complex from solution, resulting the disappearance of low energy absorption band. Solid state absorption spectra were recorded using the precipitated solids on a quartz plate (Figure 10b). All Hg(II) - **SCTs** compounds showed a small red shift (2 to 10 nm) in absorption maximum with respect to the pristine **SCTs** thin films. No significant differences in absorption maximum were observed for **SCT-2**/Hg and **SCT-3**/Hg complex. In addition, absorption spectra of **SCT-4** were recorded at different pHs to exclude the effect of possible interaction of H<sup>+</sup> with **SCT-4**. It is found that absorption of **SCT-4** is independent of changes in pH from 1 – 7 (ESI, Figure S36). The SEM micrograph on the **SCT-4**/Hg complex (ESI, Figure S37) shows a micron-sized solid cluster that stacks up in layers.

### Charge transfer complex between SCTs and TCNQ

Formation of donor-acceptor complexes through charge transfer has been well established from electron rich p-type and electron deficient n-type materials.<sup>32-34</sup> Such strong donor-acceptor charge transfer complexes with ordered nano/microstructures are known for high electrical conductivity and used as additives in organic electronics.<sup>35-37</sup> In this work, the interaction of **SCTs** with a strong acceptor, 7,7,8,8-tetracyanoquinodimethane (TCNQ) was studied using spectroscopic techniques. Formation of TCNQ dianion (TCNQ<sup>2-</sup>) was observed at 500 nm upon mixing of **SCTs** and TCNQ in THF with quenching of neutral TCNQ band at 400 nm (Figure 11).<sup>38,39</sup> Linear terthiophene<sup>40</sup> and quaterthiophenes<sup>41</sup> were known to form weak charge transfer complexes with TCNQ, resulting in low absorbance at 750 and 840 nm (TCNQ monoanion, TCNQ<sup>1-</sup>). Recently, formation of sexithiophene-TCNQ charge transfer complex with a small net charge transfer was reported.<sup>42,43</sup> In contrast, the highly branched **SCTs** showed full conversion of TCNQ to TCNQ<sup>2-</sup>, which suggested strong charge transfer from **SCTs** to TCNQ. Optical titration studies were carried out to investigate the concentration effect of **SCTs** on formation of TCNQ dianion (TCNQ<sup>2-</sup>) in THF (Figure 12 and 13). As shown in Figure 13c, low concentration of **SCT-4** (4 meq) shows immediate quenching of neutral TCNQ absorption band. In contrast, presence of neutral TCNQ band was observed in **SCT-1** and **SCT-2** even at high concentration (Figure 12a and c). This suggests **SCT-4** is strongly electron-donating and the charge transfer to TCNQ is more efficient. The observed quenching of emission from **SCTs** upon titration with TCNQ were explained due to the formation of ground state charge transfer complex of **SCTs** and TCNQ.

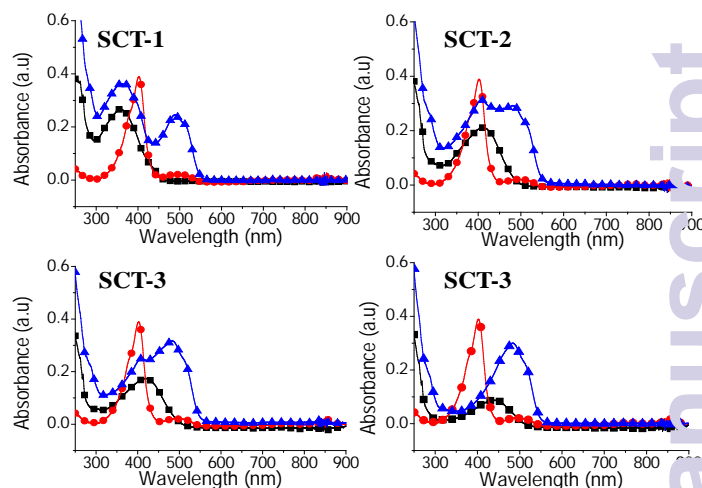


**Figure 11.** Solution state absorption spectra of pristine **SCTs** (■) and TCNQ (●),  $6.0 \times 10^{-5}$  M, and after mixing in THF (▲).

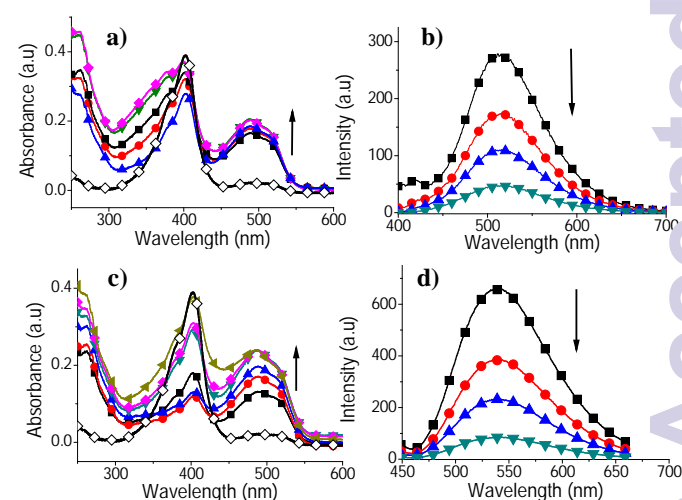


**Figure 12.** (a) Absorption spectra of TCNQ (◇), upon titration with **SCT-1** (70 meq (■), 140 meq (●), 210 meq (▲), 280 meq (▼), and 350 meq (◆) in THF; and (b) emission spectra of **SCT-1** (■) upon titration of TCNQ (8 eq (●), 16 eq (▲), and 32 eq (▼) in THF; c) Absorption spectra of TCNQ (◇), upon titration with **SCT-2** (7 meq (■), 23 meq (●), 33 meq (▲), 43 meq (▼), and 53 meq (◆) in THF; and (d) emission spectra of **SCT-2** (■) upon titration of TCNQ (8 eq (●), 16 eq (▲), and 32 eq (▼), in THF.

A higher equivalent of TCNQ was required for quenching of emission from **SCT-4** as compared to that observed in other **SCTs** (Figure 13d). This is consistent to the absorption studies which indicate a smaller amount of **SCT-4** was sufficient to quench the neutral TCNQ absorption peak. Both absorption and photoluminescence studies indicate that **SCTs** have strong affinity towards TCNQ in the formation of charge-transfer complex.

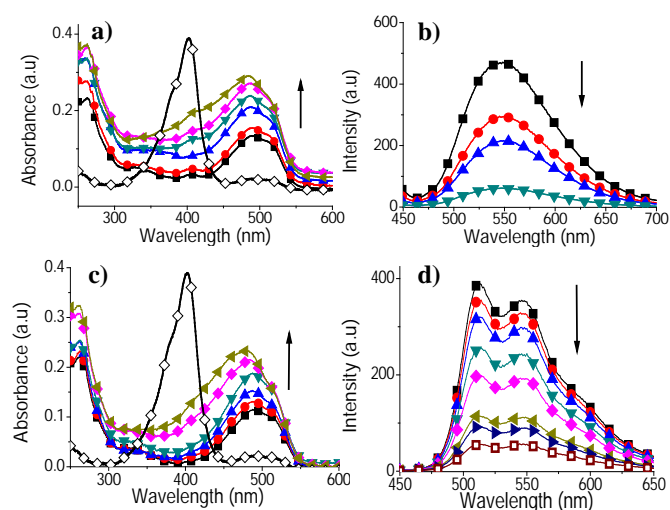


**Figure 13.** (a) Absorption spectra of TCNQ ( $\diamond$ ), upon titration with **SCT-3** (4 meq ( $\blacksquare$ ), 11 meq ( $\bullet$ ), 22 meq ( $\blacktriangle$ ), 33 meq ( $\blacktriangledown$ ), 44 meq ( $\blacklozenge$ ), and 89 meq ( $\blacktriangleleft$ ) in THF; and (b) emission spectra of **SCT-3** ( $\blacksquare$ ) upon titration of TCNQ (13 eq ( $\bullet$ ), 25 eq ( $\blacktriangle$ ), and 50 eq ( $\blacktriangledown$ ) in THF; (c) upon titration with **SCT-4** (3 meq ( $\blacksquare$ ), 7 meq ( $\bullet$ ), 13 meq ( $\blacktriangle$ ), 22 meq ( $\blacktriangledown$ ), 30 meq ( $\blacklozenge$ ), and 58 meq ( $\blacktriangleleft$ ) in THF; and (d) emission spectra of **SCT-4** ( $\blacksquare$ ) upon titration of TCNQ (64 eq ( $\bullet$ ), 128 eq ( $\blacktriangle$ ), 256 eq ( $\blacktriangledown$ ), 512 eq ( $\blacklozenge$ ), 1024 eq ( $\blacktriangleleft$ ), 1282 eq ( $\blacktriangleright$ ), and 1923 eq ( $\square$ ) in THF.

### Morphology of SCTs/TCNQ

The surface morphology of **SCTs**/TCNQ complex was studied using SEM. The solutions of **SCTs**/TCNQ in THF were dropcasted on a glass substrates and slow evaporation of the solvent gave nanosized needle or rod-shaped crystals (ESI, Figure S38). These needles were morphologically different from the pristine flat crystals of TCNQ. The high magnification SEM micrographs of the **SCT-4**/TCNQ showed needles with a diameter in the range of 140 – 180 nm. Similar organization of molecules was also reported in other TCNQ charge-transfer complexes such as CuTCNQ,<sup>44</sup> Ni[TCNQ]<sub>2</sub>(H<sub>2</sub>O)<sub>2</sub>,<sup>45</sup> and [TTF][TCNQ]<sup>46</sup> (TTF: tetrathiafulvalene).

### Conclusions

In summary, a series of multi-dimensional branched oligothiophenes with different conjugation lengths was synthesized and characterized using different techniques. All compounds were soluble in common organic solvents. **SCTs** showed a red-shift in absorption maxima as number of thiophene units increases from **SCT-1** ( $\lambda_{\text{max}} = 360$  nm) to **SCT-2** ( $\lambda_{\text{max}} = 410$  nm), **SCT-3** ( $\lambda_{\text{max}} = 413$  nm), and **SCT-4** ( $\lambda_{\text{max}} = 440$  nm) in THF. Both optical and electrochemical studies suggest a non-planar conformation for structurally rigid **SCTs**. Electron deficient molecules such as TCNQ and heavy metal cations interact strongly with electron rich oligothiophenes. Hg(II) cations completely quenched the photoluminescence intensity of **SCT-4** through charge-transfer complex formation. Optical studies suggest that the formation of ground state **SCTs**-TCNQ

charge transfer complex is favored. Such materials with good solubility, high thermal stability, controlled micro/nanostructures and strong electron donating property will be useful in various applications.

### Experimental

#### Materials

All chemicals and reagents were purchased from commercial sources (Sigma Aldrich, Alfa Aesar and Merck) and used without further purification. Reactions were monitored by thin-layer chromatography (TLC) carried out on silica gel plates. Preparative separations were performed by column chromatography using silica gel grade 60 (0.040 – 0.063 mm) from Silicycle.

#### Instrumentation

<sup>1</sup>H NMR and <sup>13</sup>C NMR spectra were recorded on Bruker Avance AV300 (300 MHz) and Bruker Avance AV500 (500 MHz) NMR instruments using appropriate deuterated solvents from Cambridge Isotope Laboratories. The chemical shifts were reported in part per million or ppm and referenced to the residual solvent peak: s = singlet, d = doublet, t = triplet, m = multiplet, and br = broad. Electron Impact mass spectroscopy (EI-MS) high resolution mass spectra were obtained on a Finnigan TSQ7000. Elemental analysis was carried out on Elementar Vario Micro Cube. Matrix assisted laser desorption ionization-Time of Flight (MALDI-TOF) mass spectra were recorded on a Bruker Autoflex III TOF/TOF with reflectron analyzers in positive ionization mode. UV-visible spectra were measured on a UV-1800 Shimadzu UV-VIS spectrophotometer with an optical filter that is calibrated at a bandwidth of 1 nm. The emission spectra were measured on a RF-5301PC Shimadzu spectrofluorophotometer with appropriate analytical grade solvents. The cyclic voltammograms were recorded with a computer controlled CHI electrochemical analyzer at a constant scan rate of 100 mV/s. The potentials were calibrated using ferrocene/ferrocenium ion redox couple as internal reference. The onset of oxidation ( $E_{\text{ox}}^{\text{onset}}$ ) and reduction ( $E_{\text{red}}^{\text{onset}}$ ) were used to estimate HOMO ( $E_{\text{HOMO}}$ ) and LUMO ( $E_{\text{LUMO}}$ ) energy levels of polymers using the equation  $E_{\text{HOMO}} = -(4.8 + E_{\text{ox}}^{\text{onset}})$  and  $E_{\text{LUMO}} = -(4.8 + E_{\text{red}}^{\text{onset}})$ . Structural optimization and frontier orbital energy levels were calculated using density functional (DFT) level at B3LYP/6-31G(d) level. The LUMO and HOMO electron density plots were generated from the optimized structures using Gaussview 5. Thermogravimetric analysis (TGA) was recorded under nitrogen atmosphere using a heating rate of 10 °C min<sup>-1</sup> on a TA Instruments 2960. Differential Scanning Calorimetry (DSC) data were recorded under nitrogen atmosphere using Mettler Toledo DSC1. All samples (3 mg) were dried at 50 °C under vacuum for 24 hours to remove residual moisture prior to thermal analysis. Scanning electron micrographs were recorded using a JEOL JSM-6701F Field Emission Scanning Electron Microscope (SEM).

**Synthesis of materials and sample preparation**

**3,3'-Dibromo-2,2'-bithiophene (1):** 3-Bromothiophene (10.4 g, 63.8 mmol) was dissolved in anhydrous THF (80 mL) under nitrogen atmosphere. The reaction mixture was cooled to -78 °C followed by the slow addition of 2M lithium diisopropylamide solution (33.6 mL, 67.0 mmol) over 30 minutes. The reaction mixture was stirred at -78 °C for an hour. CuCl<sub>2</sub> (17.1 g, 127.2 mmol) was added in one portion and continued to stir for 10 minutes before it was allowed to warm up to room temperature. After all starting materials had been consumed (monitored by TLC), dilute HCl was added to the reaction mixture, and the product was extracted with diethyl ether (2 x 100 mL). The organic layer was washed with brine solution and water, dried over anhydrous sodium sulfate and concentrated under reduced pressure. The crude product was purified on a silica gel column using hexane as eluent to give a pale-yellowish liquid (11.8 g, yield 57%). <sup>1</sup>H NMR (300 MHz, CDCl<sub>3</sub>, δ ppm) 7.41 (d, 2H, J = 5.4 Hz), 7.08 (d, 2H, J = 5.4 Hz). <sup>13</sup>C NMR (75 MHz, CDCl<sub>3</sub>, δ ppm) 130.75, 128.83, 127.48, 112.58. MS (EI): M<sup>+</sup> (C<sub>8</sub>H<sub>4</sub>Br<sub>2</sub>S<sub>2</sub>) Calculated m/z = 323.8, Found m/z = 323.8.

**3,3':2,2':3,3'''-Quaterthiophene (2):** Compound **1** (3.51 g, 10.8 mmol), 3-thiophene boronic acid (3.05 g, 23.8 mmol), and Pd(PPh<sub>3</sub>)<sub>4</sub> (0.50 g, 0.4 mmol) were dissolved in pre-degassed mixture of THF (20 mL) and 2M aqueous K<sub>2</sub>CO<sub>3</sub> (8 mL) solution. The reaction mixture was refluxed for 24 hours, cooled, diluted with water (100 mL), and extracted with ethyl acetate (2 x 100 mL). The combined organic fraction was washed with brine solution and water, dried over anhydrous sodium sulfate, and concentrated under reduced pressure. The crude product was purified on silica gel column using a mixture of 5% ethyl acetate in hexane as eluent to yield a white solid (1.63 g, yield 45%). <sup>1</sup>H NMR (300 MHz, CD<sub>2</sub>Cl<sub>2</sub>, δ ppm) 7.48(d, 2H, J = 5.3 Hz), 7.33 (d, 2H, J = 5.3 Hz), 7.21 (dd, 2H, J = 5.0, 3.0 Hz), 7.09 (dd, 2H, J = 3.0, 1.3 Hz), 7.00 (dd, 2H, J = 5.0, 1.3 Hz). <sup>13</sup>C NMR (75 MHz, CDCl<sub>3</sub>, δ ppm) 136.68, 136.20, 128.95, 128.54, 127.18, 126.70, 125.19, 122.04. HRMS (EI): M<sup>+</sup> (C<sub>16</sub>H<sub>10</sub>S<sub>4</sub>) Calculated m/z = 329.9665, Found m/z = 329.9665. Anal. Calcd. for C<sub>16</sub>H<sub>10</sub>S<sub>4</sub>: C, 58.14; H, 3.05; S, 38.8. Found: C, 58.28; H, 3.03; S, 38.62%.

**(3):** N-Bromosuccinimide (11.4 g, 64 mmol) was added slowly to a solution of **2** (1.63 g, 4.9 mmol) in CHCl<sub>3</sub> (20 mL) and acetic acid (60 mL) at room temperature. The reaction mixture was stirred at 80 °C for 4 hours. After cooling to room temperature, the reaction mixture was neutralized with aqueous NaOH solution and extracted with CHCl<sub>3</sub> (2 x 50 mL). The combined organic fraction was washed with brine solution and water, dried over anhydrous sodium sulfate, and concentrated under reduced pressure. The crude solid was purified on a silica gel column using 5% DCM in hexane as eluent to yield a pale yellow solid (2.2 g, yield 56%). <sup>1</sup>H NMR (300 MHz, CDCl<sub>3</sub>, δ ppm) 7.05 (s, 2H), 6.38 (s, 2H). <sup>13</sup>C NMR (75 MHz, CDCl<sub>3</sub>, δ ppm) 135.26, 132.79, 132.38, 130.49, 113.21, 111.64, 109.94, 104.95. HRMS (EI): M<sup>+</sup> (C<sub>16</sub>H<sub>4</sub>Br<sub>6</sub>S<sub>4</sub>) Calculated m/z = 803.4235, Found m/z = 803.4255. Anal. Calcd. for

C<sub>16</sub>H<sub>4</sub>Br<sub>6</sub>S<sub>4</sub>: C, 23.91; H, 0.50; S, 15.95. Found: C, 23.97; H, 0.54; S, 15.89%.

**SCT-1:** Compound **3** (0.22 g, 0.27 mmol) and Pd(PPh<sub>3</sub>)<sub>4</sub> (0.03 g, 0.03 mmol) were dissolved in anhydrous THF (12 mL) under nitrogen atmosphere. 2-(Tributylstannyl)thiophene (1.04 mL, 3.28 mmol) was added via syringe and the reaction mixture was stirred under reflux for 38 hours. After cooling to room temperature, the reaction mixture was added to chloroform (50 mL), washed with 5M HCl (50 mL), water (50 mL), saturated NaHCO<sub>3</sub> solution (25 mL), brine solution, and water. The organic fraction was dried over anhydrous sodium sulfate and the excess solvent was removed under reduced pressure. The crude solid was purified on a silica gel column using 5% DCM in hexane as eluent to give pale-yellow solid (0.17 g, yield 75%). <sup>1</sup>H NMR (300 MHz, CDCl<sub>3</sub>, δ ppm) 7.19 (dd, 2H, J = 5.1, 1.1 Hz), 7.16 (dd, 2H, J = 5.1, 1.1 Hz), 7.12 (m, 2H), 7.08 (dd, 2H, J = 3.6, 1.1 Hz), 7.02 (dd, 2H, J = 3.7, 0.9 Hz), 6.99 (dd, 2H, J = 5.1, 3.7 Hz), 6.96 (s, 2H), 6.94 (dd, 2H, J = 5, 3.6 Hz), 6.86 (s, 2H), 6.85 (d, 2H, J = 1.1 Hz), 6.78 (s, 2H). <sup>13</sup>C NMR (126 MHz, CDCl<sub>3</sub>, δ ppm) 137.50, 136.87, 136.84, 135.34, 135.32, 134.07, 132.72, 132.57, 131.47, 127.82, 127.72, 127.11, 126.27, 125.85, 125.82, 125.67, 125.61, 124.64, 124.31, 123.80, 123.56. HRMS (EI): M<sup>+</sup> (C<sub>40</sub>H<sub>22</sub>S<sub>10</sub>) Calculated m/z = 821.8929, Found m/z = 821.8959. Anal. Calcd. for C<sub>40</sub>H<sub>22</sub>S<sub>10</sub>: C, 58.36; H, 2.69; S, 38.95 Found: C, 58.48; H, 2.65; S, 38.81%.

**SCT-2:** Compound **3** (0.13 g, 0.16 mmol), 2,2'-bithiophene-5-boronic acid pinacol ester (0.48 g, 1.60 mmol) and Pd(PPh<sub>3</sub>)<sub>4</sub> (0.04 g, 0.03 mmol) were dissolved in a mixture of THF (8 mL), 2M aqueous K<sub>2</sub>CO<sub>3</sub> solution (2mL) under nitrogen atmosphere. The reaction mixture was degassed with nitrogen for 10 minutes and stirred under reflux for 38 hours. The work up is same as described for **SCT-1**. The crude solid obtained was washed with acetone to remove any unreacted reagents and impurities. The solid was again dissolved in chloroform and precipitated repeatedly in MeOH/ 5M HCl (80 : 20) mixture to yield a bright orange solid (0.13 g, yield 60%). <sup>1</sup>H NMR (300 MHz, THF-d<sub>8</sub>, δ ppm) 7.33 (dd, 2H, J = 5.2, 1.1 Hz), 7.30 (dd, 2H, J = 5.2, 1.2 Hz), 7.23 (dd, 2H, J = 5.1, 1.1 Hz), 7.22 (dd, 2H, J = 3.6, 1.1 Hz), 7.20 (dd, 2H, J = 3.6, 1.1 Hz), 7.18 (s, 2H), 7.11 (dd, 2H, J = 3.6, 1.1 Hz), 7.08 (d, 2H, J = 3.8 Hz), 7.04 (d, 2H, J = 3.4 Hz), 7.01 - 6.97 (4H), 6.94 (d, 2H, J = 3.8 Hz), 6.92 - 6.87 (6H), 6.86 (s, 2H), 6.71 (d, 2H, J = 3.8 Hz). <sup>13</sup>C NMR (126 MHz, THF-d<sub>8</sub>, δ ppm) δ 139.06, 138.93, 137.76, 137.66, 137.63, 137.44, 137.00, 136.40, 136.14, 136.12, 136.06, 135.14, 134.11, 131.97, 128.52, 128.46, 128.37, 127.63, 126.57, 126.55, 125.41, 125.32, 125.23, 125.19, 125.02, 125.00, 124.90, 124.63, 124.48, 124.45, 124.34. MALDI-TOF: (C<sub>64</sub>H<sub>34</sub>S<sub>16</sub>) Calculated m/z = 1316.0, Found m/z = 1316.2. Anal. Calcd. for C<sub>64</sub>H<sub>34</sub>S<sub>16</sub>: C, 58.41; H, 2.60; S, 38.98, Found: C, 58.41; H, 2.50; S, 38.78%.

**SCT-3:** Compound **3** (0.22 g, 0.27 mmol), 5'-hexyl-2,2'-bithiophene-5-boronic acid pinacol ester (1.03 g, 2.70 mmol) and Pd(PPh<sub>3</sub>)<sub>4</sub> (0.09 g, 0.08 mmol) were dissolved in a mixture of THF (8 mL), 2M aqueous K<sub>2</sub>CO<sub>3</sub> solution (2 mL) under

nitrogen atmosphere. The work up is same as described for **SCT-1**. The crude product was purified on a silica gel column using a mixture of 5% chloroform in hexane followed by precipitation in MeOH to yield an orange solid (0.19 g, yield 38%).  $^1\text{H}$  NMR (300 MHz,  $\text{CDCl}_3$ ,  $\delta$  ppm) 7.00 (s, 2H), 6.95 (d, 2H,  $J = 3.5$  Hz), 6.94 - 6.92 (m, 4H), 6.89 (d, 2H,  $J = 3.3$  Hz), 6.83 - 6.78 (m, 6H), 6.76 - 6.74 (m, 2H), 6.71 - 6.63 (m, 6H), 6.60 (d, 2H,  $J = 3.5$  Hz), 6.54 (d, 2H,  $J = 3.3$  Hz), 2.80 (t, 8H,  $J = 7.2$  Hz), 2.71 (t, 4H,  $J = 7.2$  Hz), 1.65 (m, 12 H), 1.32 (m, 36 H), 0.91 - 0.89 (m, 18H).  $^{13}\text{C}$  NMR (126 MHz,  $\text{CDCl}_3$ ,  $\delta$  ppm) 145.61, 145.38, 145.31, 138.50, 138.20, 137.13, 136.57, 135.50, 134.93, 134.87, 134.65, 134.52, 134.49, 134.16, 133.38, 132.87, 131.18, 131.08, 126.57, 125.52, 125.45, 124.81, 124.75, 124.66, 124.40, 124.01, 123.51, 123.48, 123.40, 123.37, 123.26, 123.19, 31.58, 31.56, 31.48, 30.23, 30.20, 30.16, 29.69, 28.84, 28.82, 28.76, 22.59, 22.56, 14.08, 14.06. MALDI-TOF: ( $\text{C}_{100}\text{H}_{106}\text{S}_{16}$ ) Calculated  $m/z = 1820.4$ , Found  $m/z = 1820.9$ . Anal. Calcd. for  $\text{C}_{100}\text{H}_{106}\text{S}_{16}$ : C, 65.96; H, 5.87; S, 28.17. Found: C, 65.69; H, 6.00; S, 28.05%.

**SCT-4:** Compound **3** (0.16 g, 0.2 mmol), and  $\text{Pd}(\text{PPh}_3)_4$  (0.03 g, 0.03 mmol) were dissolved in anhydrous THF (12 mL) under nitrogen atmosphere. 5-(Tributylstannyl)-5''-hexyl-2,2':5,2''-terthiophene (1.00 g, 1.6 mmol) was added via the syringe and the reaction mixture was stirred under reflux for 48 hours. The work up is same as described for **SCT-1**. The crude solid was washed with acetone to remove any unreacted reagents and impurities. The solid was dissolved in chloroform and precipitated from MeOH/ 5M HCl (80 : 20) mixture to yield an orange solid (0.22 g, yield 47%). Due to the poor solubility of **SCT-4** in common solvents, we were unable to get a good  $^{13}\text{C}$  NMR spectrum.  $^1\text{H}$  NMR (300 MHz,  $\text{THF-d}_8$ ,  $\delta$  ppm) 7.25 - 7.12 (m, 5H), 7.11 - 6.76 (m, 26 H), 6.75 - 6.50 (m, 9H), 2.78 (m, 12H), 1.63 (m, 12 H), 1.32 (m, 36H), 0.90 (m, 18H). MALDI-TOF: ( $\text{C}_{124}\text{H}_{118}\text{S}_{22}$ ) Calculated  $m/z = 2312.3$ , Found  $m/z = 2312.8$ . Anal. Calcd. for  $\text{C}_{124}\text{H}_{118}\text{S}_{22}$ : C, 64.37; H, 5.14; S, 30.49. Found: C, 64.14; H, 5.18; S, 30.21%.

#### Preparation of SCTs stock solutions

Dilute solutions of **SCTs** were prepared by dissolving appropriate amounts of **SCTs** in HPLC grade THF. The solution was sonicated for 30 minutes to make sure all solids were fully dissolved and used for further studies. The concentrations for **SCT-1**, **SCT-2**, **SCT-3** and **SCT-4** were  $1.3 \times 10^{-4}$  M,  $6.0 \times 10^{-5}$  M,  $4.0 \times 10^{-5}$  M, and  $2.6 \times 10^{-5}$  M, respectively.

#### Sample preparations for morphology studies of SCTs

Appropriate amount of stock solution of **SCTs** (100  $\mu\text{L}$ ) was taken and diluted to 1.0 mL with THF, which was added slowly to 1.0 mL of  $\text{H}_2\text{O}$  in a glass vial with screw cap. The above solution was left at room temperature for two days. The resulting solid was transferred to a glass substrate and dried under ambient condition before examination by FESEM.

#### Sample preparations for photophysical studies of SCTs/Hg(II)

To **SCTs** solution (200  $\mu\text{L}$ ), appropriate amount of mercury(II) acetate dissolved in deionized water was added, and the resulting solution was diluted with THF to make up a total volume of 1.0 mL prior to spectroscopic studies. For example, 200  $\mu\text{L}$  of the **SCT-4** was added with 20  $\mu\text{L}$  of mercury(II) acetate in deionized water (0.05 M), and the solution was diluted with THF to a final volume of 1.0 mL.

#### Sample preparations for photophysical studies of SCTs/TCNQ

Stock solution ( $6.0 \times 10^{-5}$  M) of TCNQ was prepared in THF and appropriate volume (300  $\mu\text{L}$ ) of solution was mixed with desired amount of **SCTs** and diluted with THF to make up a total volume of 2.0 mL prior to spectroscopic studies.

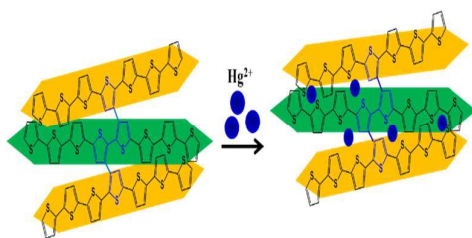
#### Acknowledgements

We would like to thank Department of Chemistry, National University of Singapore (NUS) for funding and technical supports, and NUS high performance computing centre for computations.

#### Notes and references

- J. L. Segura, N. Martin, D. M. Guldi, *Chem. Soc. Rev.* 2005, **34**, 31-47.
- M. T. Dang, L. Hirsch, G. Wantz, *Adv. Mater.* 2011, **23**, 3597 - 3602.
- G. Gigli, O. Inganäs, M. Anni, M. De Vittorio, R. Cingolani, G. Barbarella, L. Favaretto, *Appl. Phys. Lett.* 2001, **78**, 1493-1495.
- M. Melucci, M. Zambianchi, L. Favaretto, V. Palermo, E. Treossi, M. Montalti, S. Bonacchi, M. Cavallini, *Chem. Commun.* 2011, **47**, 1689-1691.
- G. Horowitz, M. E. Hajlaoui, *Adv. Mater.* 2000, **12**, 1046-1050.
- J. G. Mei, K. R. Graham, R. Stalder, S. P. Tiwari, H. Cheun, J. Shim, M. Yoshio, C. Nuckolls, B. Kippelen, R. K. Castellano, J. R. Reynolds, *Chem. Mater.* 2011, **23**, 2285-2288.
- R. P. Ortiz, J. Casado, V. Hernández, J. T. L. Navarrete, J. A. Letizia, M. A. Ratner, A. Facchetti, T. J. Marks, *Chem. Eur. J.* 2009, **15**, 5023-5039.
- M. Halik, H. Klauk, U. Zschieschang, G. Schmid, S. Ponomarenko, S. Kirchmeyer, W. Weber, *Adv. Mater.* 2003, **15**, 917-922.
- F. Laquai, D. Andrienko, R. Mauer, P. W. M. Blom, *Macromol. Rapid Commun.* 2015, **36**, 1001-1025.
- A. Mishra, C. -Q. Ma, P. Bäuerle, *Chem. Rev.* 2009, **109**, 1141 - 1276.
- Z. Li, J. Bian, Y. Wang, F. Jiang, G. Liang, P. He, Q. Hou, J. Tong, Y. Liang, Z. Zhong, Y. Zhou, W. Tian, *Sol. Energy Mater. Sci. Cells* 2014, **130**, 336-346.
- S. C. Lan, C. K. Chang, Y. H. Lu, S. W. Lin, A. K. Y. Jen, K. H. Wei, *RSC Adv.* 2015, **5**, 67718-67726.
- R. Shoumura, K. Sugiyasu, T. Yasuda, A. Sato, M. Takeuchi, *Macromolecules* 2012, **45**, 3759-3771.
- L. Guan, P. Liu, *J. Nanosci. Nanotechnol.* 2015, **15**, 3029-3034.
- J. Luo, K. W. Huang, H. M. Qu, X. J. Zhang, L. J. Zhu, H. S. J. Chan, C. Y. Chi, *Org. Lett.* 2010, **12**, 5660-5663.
- V. Jeux, C. Dalinot, M. Allain, L. Sanguinet, P. Leriche, *Tetrahedron Lett.* 2015, **56**, 1383-1387.
- C. J. Xia, X. W. Fan, J. Locklin, R. C. Advincula, *Org. Lett.* 2002, **4**, 2067-2070.

- 18 F. Huang, K. S. Chen, H. L. Yip, S. K. Hau, O. Acton, Y. Zhang, J. D. Luo, A. K. Y. Jen, *J. Am. Chem. Soc.* 2009, **131**, 13886-13887.
- 19 A. Bilge, A. Zen, M. Forster, H. Li, F. Galbrecht, B. S. Nehls, T. Farrell, D. Neher and U. Scherf, *J. Mater. Chem.* 2006, **16**, 3177-3182.
- 20 A. Zen, A. Bilge, F. Galbrecht, R. Alle, K. Meerholz, J. Grenzer, D. Neher, U. Scherf, T. Farrell, *J. Am. Chem. Soc.* 2006, **128**, 3914-3915.
- 21 M. Tateno, M. Takase, M. Iyoda, K. Komatsu, T. Nishinaga, *Chem Eur. J.* 2013, **19**, 5457 – 5467.
- 22 S. Klod, K. Haubner, E. Jähne, L. Dunsch, *Chem Sci.* 2010, **1**, 743 – 750.
- 23 S. Gronowitz, *Acta Chem. Scand.* 1961, **15**, 1393-1395.
- 24 N. Jayasuriya, J. Kagan, D. Huang, B. Teo, *Heterocycles* 1988, **27**, 1391-1394.
- 25 C. Taliani, W. Gebauer in *Handbook of Oligo- and Polythiophenes*, Wiley-VCH Verlag GmbH, 2007, pp. 361-404.
- 26 D. D. Cunningham, L. Laguren-Davidson, H. B. Mark, C. Van Pham, H. Zimmer, *J. Chem. Soc., Chem. Commun.* 1987, 1021-1023.
- 27 F. Charra, D. Fichou, J. M. Nunzi, N. Pfeffer, *Chem. Phys. Lett.* 1992, **192**, 566-570.
- 28 J. P. Parakka, J. A. Jeevarajan, A. S. Jeevarajan, L. D. Kispert, M. P. Cava, *Adv. Mater.* 1996, **8**, 54-59.
- 29 A. F. D. de Namor, I. Abbas, *J. Phys. Chem. B* 2007, **111**, 5803-5810.
- 30 A. Pal, B. Bag, *J Photochem Photobiol A* 2012, **240**, 42-49.
- 31 R. Castañeda, V. N. Khrustalev, A. Fonari, J-L. Bredas, Y. A. Getmanenko, T. V. Timofeeva, *J. Mol. Struct.* 2015, **1100**, 506-512
- 32 N. S. Sariciftci, L. Smilowitz, A. J. Heeger, F. Wudl, *Science* 1992, **258**, 1474-1476.
- 33 K. Kim, J. Liu, M. A. G. Namboothiry, D. L. Carroll, *Appl. Phys. Lett.* 2007, **90**, 163511.
- 34 X. Han, Z. Wu, B. Sun, *Org. Electron.* 2013, **14**, 1116-1121.
- 35 J. K. Jeszka, J. Ulański, M. Kryszewski, *Nature* 1981, **289**, 390-391.
- 36 H. Kobayashi, J. Nakayama, *Bull. Chem. Soc. Jpn.* 1981, **54**, 2408-2411.
- 37 T. Sumimoto, K. Kudo, T. Nagashima, S. Kuniyoshi, K. Tanaka, *Synth. Met.* 1995, **70**, 1251-1252.
- 38 H. T. Jonkman, J. Kommandeur, *Chem. Phys. Lett.* 1972, **15**, 496-499.
- 39 Y. H. Kim, S. D. Jung, M. A. Chung, K. D. Song, D. W. Cho, *Bull. Korean Chem. Soc.* 2008, **29**, 948-952.
- 40 B. Xu, D. Fichou, G. Horowitz, F. Garnier, *Synth. Met.* 1991, **42**, 2319-2322.
- 41 S. Hotta, K. Waragai, *Synth. Met.* 1989, **32**, 395-397.
- 42 F. Jäckel, U. G. E. Perera, V. Iancu, K. F. Braun, N. Koch, J. P. Rabe, S. W. Hla, *Phys. Rev. Lett.* 2008, **100**, 126102.
- 43 K. F. Braun, S. W. Hla, *J. Chem. Phys.* 2008, **129**, 064707.
- 44 S. Pal, S. Maiti, U. N. Maiti, K. K. Chattopadhyay, *J. Mater. Chem. C* 2014, **2**, 4005-4011.
- 45 J. Song, Z. Ji, Q. Nie, W. Hu, *Nanoscale* 2014, **6**, 2573-2576.
- 46 J. P. Savy, D. de Caro, C. Faulmann, L. Valade, M. Almeida, T. Koike, H. Fujiwara, T. Sugimoto, J. Fraxedas, T. Ondarcuhu, C. Pasquier, *New J. Chem.* 2007, **31**, 519-527.



A series of new branched 3D oligothiophenes with enhanced solubility are synthesized and studied. The extension in conjugation of oligothiophenes can be easily achieved. The formation of charge transfer complexes of oligothiophenes with Hg(II) ions and TCNQ is observed in solution state.